Hydrol. Earth Syst. Sci. Discuss., 11, 10431–10463, 2014
www.hydrol-earth-syst-sci-discuss.net/11/10431/2014/
doi:10.5194/hessd-11-10431-2014

Hydrology and Earth System Sciences
Open Access
Discussions

Diagnosing the seasonal land–atmosphere coupling strength over Northern Australia: dependence on soil moisture state and coupling strength definition

M. Decker, A. Pitman, and J. Evans

Climate Change Research Centre and ARC Centre of Excellence for Climate System Science, University of New South Wales, Sydney, Australia

Received: 21 July 2014 – Accepted: 26 August 2014 – Published: 19 September 2014

Correspondence to: M. Decker (m.decker@unsw.edu.au)

Published by Copernicus Publications on behalf of the European Geosciences Union.

Abstract

The strength of land–atmosphere coupling during the onset (September) through to the peak (February) of the wet season over Northern Australia is statistically diagnosed using ensembles of land surface model simulations that produce a range of different background soil moisture states. We derive coupling strength between the soil moisture and the planetary boundary layer via a statistical measure of association. The simulated evaporative fraction and the boundary layer are shown to be strongly coupled during both SON and DJF despite the differing background soil moisture states between the two seasons as among the ensemble members. The sign and magnitude of the surface layer soil moisture based coupling strength during the onset of the wet season (SON) differs from the coupling between the evaporative fraction and boundary layer from the same season, and the coupling between the surface soil moisture and boundary layer coupling during DJF. The patterns and magnitude of the surface flux-boundary layer coupling are not captured when coupling is diagnosed using the surface layer soil moisture alone. The conflicting results arise because the surface layer soil moisture lacks strong association with the atmosphere during the monsoon onset because the evapotranspiration is dominated by transpiration. Our results indicate that accurately diagnosing coupling strength in seasonally dry regions, such as Northern Australia, requires root zone soil moisture to be included.

1 Introduction

The land surface influences the atmosphere at multiple spatial and temporal scales (Pitman, 2003; Pielke et al., 2011; Williams and Maxwell, 2011). Land-atmosphere coupling strength is the degree to which land surface anomalies (e.g. soil moisture, vegetation characteristics, temperature, snow cover) lead to changes in atmospheric states and fluxes (e.g. rainfall, cloud cover, moisture convergence) as well as how anomalies in the atmosphere affect the land surface. The influence of land surface anomalies on

HESSD
11, 10431–10463, 2014

atmospheric anomalies (and vice versa) proceeds through a chain of non-linear processes. The strength of these processes varies spatially and temporally and depend, in part, on the background state of the system (Betts, 2004; Koster and Suarez, 2003; Taylor and Ellis, 2006). The chain of mechanisms between soil moisture (SM) and precipitation (P) anomalies can be summarized following Santanello et al. (2011) as

$$\Delta SM \Rightarrow \Delta EF_{SM} \Rightarrow \Delta PBL \Rightarrow \Delta EF_{ATM} \Rightarrow \Delta CLD \Rightarrow \Delta P \quad (1)$$

where the changes in soil moisture (ΔSM) lead to changes in evaporative fraction (ΔEF_{SM}), which alters the properties of the planetary boundary layer (ΔPBL) including the state (temperature, humidity) and the entrainment rate. These three near surface coupling mechanisms (ΔSM, ΔEF_{SM}, and ΔPBL) precede changes away from the land surface that further change evaporative fraction (ΔEF_{ATM}), leading to changes in cloud development and growth (ΔCLD), and ultimately forcing changes in precipitation (ΔP). The chain cycles with ΔP driving ΔSM to varying degrees depending on the region and season (Zhang et al., 2008). Equation (1) is a conceptualization of complex and non-linear processes, such that the sign of the ΔCLD response to a ΔSM forcing can vary (Westra et al., 2012; Gentine et al., 2013). Equation (1) is a simplification of the short (less than a day) timescale coupling mechanisms. Large or decadal scale processes, such as the response of vegetation to P (or P to vegetation) (Betts et al., 1996), or large scale circulation and moisture feedbacks (Lee et al., 2012; Lintner and Neelin, 2009; Lintner et al., 2013) are neglected. Additional feedbacks that operate on short timescales not shown in Eq. (1), such as ΔEF_{SM} or ΔEF_{ATM} leading to ΔSM, may also be important (Seneviratne et al., 2010; Meng et al., 2014). Despite simplifications, Eq. (1) highlights the primary control SM exerts on EF as compared to secondary factors such as entrainment (Gentine et al., 2011). In a convective regime ΔSM initiates a series of events that first alter the atmosphere (ΔPBL) prior to changing P. The series of events from ΔSM–ΔPBL comprises the terrestrial portion of the coupling mechanisms is the focus of this study, with coupling examined here limited to these

HESSD
11, 10431–10463, 2014

processes. The ΔSM through ΔPBL sequence is a necessary, but not sufficient, set of processes that determine how P responds to changes in SM.

The sensitivity of ΔP to ΔSM has been quantified with observations (Koster et al., 2003; Taylor and Ellis, 2006) and multiple model experiments. The first phase of the Global Land Atmosphere Coupling Experiment (GLACE) identified several regional "hot spots" during boreal summer where SM was strongly coupled to P with increased SM leading to increased P (Guo et al., 2006; Koster et al., 2006). The realism of these "hot spots" has not been demonstrated using observations, although the models used to simulate these "hot spots" have been validated with station measurements from several locations (Dirmeyer et al., 2006). Simulations indicate that land–atmosphere coupling can amplify P variance when the near surface humidity is high and the evaporative fraction depends on SM (Koster et al., 2000). The second phase of GLACE quantified the ability of SM anomalies to affect the temperature and P in sub-seasonal forecasts. These experiments demonstrated the asymmetric response of changes in forecast skill to the sign of the SM anomalies (Koster et al., 2011). GLACE-2 like experiments over Australia also exhibit asymmetry in the impact of coupling strength on maximum and minimum temperatures (Hirsch et al., 2013).

Alternate efforts have examined only a subset of the dynamics processes conceptualized in Eq. (1). Lee et al. (2012) turned off transpiration in a coupled land–atmosphere model to show that extreme precipitation is reduced owing to transpiration over tropical regions. In contrast to examining how moisture fluxes from the root zone alter coupling, Ferguson et al. (2012) combined multiple sources of reanalysis data with lifting condensation level (LCL) and SM observations to examine the relationship between early morning surface layer SM (SM_1), and both the LCL and the EF in the afternoon during the convective season. The relationship was quantified using the Kendall tau coefficient ($K\tau$), a non-parametric rank correlation coefficient that measures the association between two time series. Ferguson et al. (2012) found strong coupling ($K\tau$) between SM_1–EF, EF–LCL, and SM_1–LCL over many regions including monsoon regions such as Northern Australia. These three coupling mechanisms span the first

HESSD
11, 10431–10463, 2014

three components in Eq. (1) (ΔSM, ΔEF_{SM} and ΔPBL). While these represent only part of the processes involved in land–atmosphere coupling, they comprise a fundamental pathway by which SM anomalies drive an atmospheric response.

Several regional analyses have investigated the importance of land–atmosphere coupling in Northern Australia (Evans et al., 2011). Koster et al. (2000) showed land–atmosphere coupling increased the variance of P in both Northern and Eastern Australia. In agreement, Ferguson et al. (2012) found high correlations in SM_1–EF, EF–LCL, and SM_1–LCL during the convective (monsoon) season over the Northern savannas. These studies were limited in scope and did not explicitly explore how the coupling behaves during periods with different background climate states.

We focus on Northern Australia to examine whether coupling strength can be diagnosed from SM_1 in regions with a pronounced dry season, given the influence of groundwater on transpiration and deep SM variability (Decker et al., 2013). Northern Australia has a pronounced May to September dry season and a monsoon-driven wet season from November through February (Fig. 1a). The monsoonal climate allows us to examine the SM_1–LCL coupling as defined in Ferguson et al. (2012) in sharply contrasting seasons (Fig. 1a–d) that exhibit contrasting background soil moisture states. By examining the differences between coupling strength during the onset (defined here as SON to coincide with the initial increase in rainfall) of the wet season when soil moisture will be low, and then through to the peak (defined as DJF to coincide with the precipitation maximum) of the wet season, we aim to determine the reliability of diagnosing the terrestrial and near surface stages of land–atmosphere coupling using $K\tau$ derived from SM_1 and LCL during periods where total ET fluxes are dominated by either soil evaporation or transpiration. The coupling strength is defined here such that the land surface processes in Eq. (1) (ΔSM, ΔEF_{SM} and ΔPBL) are examined, while the sequence of events in the atmosphere (ΔCLD and ΔP) are neglected. This terrestrial derived coupling captures how ΔSM relates to state changes in the mixed layer (ΔPBL). Strong coupling as defined here is a necessary but not sufficient prerequisite for strong ΔSM–ΔP coupling. An ensemble of offline simulations using two model configurations, one

HESSD
11, 10431–10463, 2014

of which neglects groundwater and therefore contains greatly reduced deep soil moisture, are driven using four forcing datasets. The simulations provide estimates of SM_1 in addition to SM over the root zone (SM_{rz}), total ET and the ET components. Afternoon (14:00 LT) LCL is derived using the near surface atmospheric variables from the forcing datasets, and the sensitivity of the ensemble median $K\tau$ is examined for the onset and peak of the monsoon season.

This manuscript is organized as follows. The SM_1 and ET observations used for model validation and the near surface atmospheric datasets are summarized in Sect. 2. Section 3 outlines the statistical measure of association used for coupling strength, the derivation of LCL from the atmospheric data, and the model experiments used to estimate the evaporative fraction and soil moisture. The Results section consists of the SM_1–LCL and EF–LCL based coupling strength, the impact of defining coupling strength with SM_{rrz} (the root zone SM) are presented in Sect. 4. The results are explained in terms of the governing physical processes and previous research in Sect. 5.

2 Validation and model forcing data

2.1 Validation data: soil moisture and evapotranspiration

The simulated surface soil moisture (SM_1) is evaluated against the daily Advanced Microwave Scanning Radiometer-Earth Observing System (AMSR-E) L3 surface SM product. The data are derived from passive microwave measurements and available for the period 2002 to 2011 (Njoku et al., 2003). AMSR-E based SM compares favorably with in-situ measurements over Australia (Draper et al., 2009) and exhibits spatiotemporal variability consistent with land model simulations (Liu et al., 2009). To simplify the comparison with the simulated SM, the first model layer (~ 0.7 cm deep) SM is assumed comparable to SM from AMSR-E despite the uncertain effective measurement depth (approximately 1 cm) that varies with SM.

HESSD
11, 10431–10463, 2014

The simulated evapotranspiration is evaluated against three ET products. Multiple ET datasets based on different methodologies are included due to the uncertainty associated with deriving gridded moisture flux data (Jimenez et al., 2011). The Global Land Evaporation Amsterdam Methodology (GLEAM) (Miralles et al., 2011a, b), the model-tree ensemble based dataset from MPI-Jena (J2010 hereafter) (Jung et al., 2010), and the Moderate Resolution Imaging Spectrometer (MODIS) MOD16 dataset (Mu et al., 2007, 2011) are used to estimate the observed mean seasonal ET fluxes. The observed ET is estimated using the arithmetic mean of the three datasets after the GLEAM and MOD16 data are aggregated to the coarse resolution ($0.5^{\circ} \times 0.5^{\circ}$) of the J2010 data. The simulations are subsequently compared to the mean observed ET separately for the wet (December–February) and the end of the dry (September–November) seasons.

2.2 Near surface atmospheric state and flux data

The lifting condensation level (LCL see Sect. 3.2) is computed from combinations of near surface atmospheric data using two reanalysis products. Similarly, the model simulations (see Sect. 3.3) are driven using a combination of atmospheric states and fluxes from reanalysis products, a gauge based daily precipitation dataset, and a 3 hourly satellite-based precipitation product. We follow Decker et al. (2014) and utilize four forcing datasets to drive model simulations.

The two sources of temperature, humidity, wind speed, pressure, and radiative fluxes are the Global Land Data Assimilation System (GLDAS, http://disc.sci.gsfc.nasa.gov/hydrology/data-holdings, Rodell at al., 2004) and the Modern-Era Retrospective Analysis for Research and Applications (MERRA) product (Bosilovich et al., 2008). These two datasets are utilized due to the high spatial resolution of GLDAS (0.25°) and high temporal resolution of MERRA (hourly). Two forcing datasets are comprised of the uncorrected GLDAS and MERRA data interpolated to a common $0.25^{\circ} \times 0.25^{\circ}$ grid. In addition two precipitation corrected datasets developed in Decker et al. (2014) are used. The uncorrected atmospheric states and radiative fluxes from MERRA are combined

HESSD
11, 10431–10463, 2014

with P corrected via two algorithms. First, MERRA is corrected using the Australian Water Availability Project (AWAP) daily gridded precipitation data (Jones et al., 2009) to remove the monthly biases. Second, the MERRA precipitation is replaced with precipitation derived from disaggregating the daily AWAP data with the 3 hourly Tropical Rainfall Measuring Mission (TRMM) 3B42 (Huffman et al., 2007) data. These two corrected datasets have identical monthly mean precipitation but different distributions of sub-monthly precipitation.

3 Methods

3.1 Kendall τ

We evaluate the land–atmosphere coupling strength using Kendall tau ($K\tau$), a non-parametric, rank correlation statistic (Press et al., 1992). Following Ferguson et al. (2012), $K\tau$ is used to indicate the correspondence between two states important to land–atmosphere coupling. $K\tau$ does not assume linearity between the variables being compared and tests for statistical significance. $K\tau$ ranges from −1 to 1 (positive values indicate the temporal variations are synchronized), with statistical significance depending on the sample size (approximately 0.12 in this study). $K\tau$ is defined as

$$K_\tau = \frac{N_o - N_d}{0.5n(n-1)} \tag{2}$$

where N_o is the number of ordinate pairs, N_d is the number of disordinate pairs, and n is the number of observations. Ordinate pairs are pairs of numbers for which the change between them have the same sign, i.e. both are either positive or negative. $K\tau$ is calculated between the detrended three hourly modeled SM_1 during the morning and the estimated three hourly LCL from the afternoon at each grid cell for each season. The local time of SM and LCL varies because the simulations and forcing data utilize GMT. $K\tau$ is found separately for each of the eight simulated (see Sect. 3.3) estimates of SM_1

HESSD
11, 10431–10463, 2014

and the four estimates of LCL (Sect. 3.2), generating a total of 32 estimates of $K\tau$. The median $K\tau$ is found separately for the wet and dry seasons for the two different model configurations (Sect. 3.3) to give the final estimation of the coupling strength. The coupling is also diagnosed using $K\tau$ between the model simulated afternoon evaporative fraction and the afternoon LCL. A second definition of coupling is found by calculating $K\tau$ between the morning time root zone SM (SM_{rz}) and the afternoon LCL (SM_{rz}–LCL). SM_{rz} is defined as the vertically averaged SM from the surface to a depth of 1 m.

3.2 Calculation of lifting condensation level

The state of the convective atmosphere is evaluated using the lifting condensation level (LCL), defined as the height (in pressure) that a parcel reaches saturation when ascending adiabatically from the surface. While a lower LCL is favorable to convection, it is not a sufficient constraint to guarantee it. For convection to occur a parcel must reach the level of free convection (LFC), which may not occur even if a parcel reaches the LCL. The height (in pressure) of the LCL is derived using only near surface variables under the assumption that the boundary layer is well developed and therefore well mixed. Estimating the LCL from near surface variables provides heights comparable to direct observations (Ferguson and Wood, 2009). Under these assumptions, the pressure at the LCL is given by

$$\mathrm{LCL} = P_{\mathrm{srf}} - P_{\mathrm{srf}} \left(\frac{T_{\mathrm{air}}}{T_{\mathrm{dew}}} \right)^{\frac{-c_p}{R}} \tag{3}$$

where P_{srf} is the surface pressure (Pa), T_{air} is the near surface air temperature (K), T_{dew} is the near surface dew point temperature (K), R is the specific gas constant of dry air ($\mathrm{J\,K^{-1}\,kg^{-1}}$), and c_p is the specific heat of dry air at constant pressure ($\mathrm{J\,K^{-1}\,kg^{-1}}$). Four estimates of LCL are found by applying Eq. (4) to several combinations of near surface forcing data. While P_{srf} and T_{air} are directly provided by both reanalysis products, T_{dew} is calculated using the available near surface atmospheric states. The four

HESSD
11, 10431–10463, 2014

estimates of LCL are calculated with Eq. (4) by: (1) using GLDAS for pressure and both temperatures, (2) using MERRA for pressure and both temperatures, (3) using pressure from MERRA and temperatures from GLDAS, and (4) using pressure from GLDAS and temperatures from MERRA. The LCL is quality controlled by limiting LCL to be less than the surface pressure.

3.3 Simulated estimates of soil moisture and evaporative fraction

Owing to the need to evaluate the soil moisture and evaporative fraction at sub-daily timescales in computing $K\tau$, we use the community land model version 4 (CLM4, Oleson et al., 2010) to simulate the states and fluxes of water and energy using configurations documented in Decker et al. (2013, 2014). The land surface model simulations and reanalysis products allow for the terrestrial leg (DSM-DPBL in Eq. 1) to be explored explicitly. A detailed description of the groundwater configurations and modifications are given in Decker et al. (2014).

The suite of simulations is utilized to address forcing data and model configuration uncertainties in addition to exploring a large soil moisture state space. Two different configuration of CLM4 are used. The first consists of the default CLM4 (referred to as CTRL). The second (referred to as DRY) uses a modified CLM4 that replaces the two-way soil moisture coupling between the soil column and the aquifer with a free drainage bottom boundary condition. The modifications significantly reduce the soil moisture at depths below several centimeters and the ET flux during periods of low rainfall while not imparting large changes on the changes in total column water (Decker et al., 2014). The two model configurations thus enable the coupling between the atmosphere and the land surface to be examined under two differing background soil moisture states.

The CLM4 evapotranspiration is computed as the sum of the soil evaporation, the canopy evaporation and the transpiration. Transpiration is determined from the rate of photosynthesis and is, in part, a function of SM. The dependence on SM is determined by the soil water potential in each soil layer, the root distribution (prescribed by plant functional type, PFT), and the PFT dependence on water stress. The spatial distribution

HESSD
11, 10431–10463, 2014

and phenology of PFTs are specified and identical across all simulations. The C3 grass PFT sets approximately 99 % of the roots within 1 m of the surface, while approximately 90 % of the roots are within this depth for the broadleaf evergreen forest PFT.

The experiment design follows the simulations outlined in Decker et al. (2014) that have been shown to be in good agreement with observations over parts of Australia. One control (CTRL) simulation and one dry simulation are equilibrated for the period 1948–1979 using the corrected NCEP/NCAR data (Qian et al., 2006) after interpolating to the same $0.25^\circ \times 0.25^\circ$ grid as the other forcing datasets. The CTRL and DRY simulations ending in 1979 provide initial conditions for the four CTRL and four DRY simulations from 1979–2007. The model evaluation period spans the five years coincident with the SM and ET data from 2003–2007. The coupling is computed using the period 1990–2008. Both the CTRL and the DRY simulations are forced with the four forcing datasets (see Sect. 2.2): GLDAS, MERRA, MERRA.B, and MERRA.BT, generating a total of eight model simulations. The SM (from all model layers), and turbulent energy fluxes are output at three hourly intervals (coincident with the temporal resolution of the GLDAS forcing), while the remaining CLM4 output is saved as monthly means.

4 Results

4.1 Validation of simulated soil moisture and evapotranspiration

The two model configurations are separately validated against the observed soil moisture and evapotranspiration on monthly and seasonal timescales, respectively. Figure 2a shows the timeseries of the area averaged (10–15° S to 120–150° E) normalized ensemble mean first layer soil moisture from the CTRL and the DRY ensembles and the AMSR-E observed data. The simulation dynamics are evaluated using the normalized SM_1 due to the difficulties in direct comparison of simulated and observed soil moisture (Reichle and Koster, 2004). The strong seasonal cycle of soil moisture owing

HESSD
11, 10431–10463, 2014

to the monsoonal climate is evident in both the observations and the simulations. CTRL and DRY are nearly identical aside from the dry season in 2003 where the soil moisture in CTRL decreases more than that from DRY. The observed moistening of the soil following the dry seasons in Fig. 2a occurs within a month to that of the simulated moistening. The mean monthly soil moisture closely follows that of the observations and exhibits dynamic behavior independent of the model configuration.

The bias of the ensemble mean time averaged surface layer soil moisture from the eight simulations against the AMSR-E data is shown in Fig. 2b. Over large regions of Northern Australia, the simulated SM_1 is within $0.025\,mm^3\,mm^{-3}$ of AMSR-E. The difference in mean SM_1 between the two model configurations is similarly small (figure not shown). Figure 2 demonstrates that the temporal evolution (Fig. 2a) and mean state (Fig. 2b) of the simulated SM_1 are similar to the AMSR-E observations.

The seasonal mean ET is validated against the arithmetic mean of the three gridded ET products for both DJF (Fig. 3a, c, and e) and SON (Fig. 3b, d, and f). The observed DJF ET (Fig. 3e) has a strong north-south gradient with a maxima centered around 13° S–130° E. The strong north-south gradient is also present in the ensemble mean ET (Fig. 3a), however the simulations overestimate DJF ET over much of the domain. The observations show an ET of less than $50\,W\,m^{-2}$ south of 18° S while the simulations remain above $60\,W\,m^{-2}$ in this region. The mean SON ET is markedly lower compared to DJF ET in both the observations (Fig. 3f) and the simulations (Fig. 3b). Similar to DJF, both the model and the observations show a strong north-south gradient. The simulations under estimate the ET in the York Peninsula (East of 140° E and North of 17° S) during SON and overestimate the ET in this region during DJF. The underestimation of the SON ET in the simulations is largely a result of including the DRY model configuration. The CTRL simulations exhibit a 10–20 $W\,m^{-2}$ increase in SON ET over the DRY model runs (Fig. 3b and d). Overall, the model exhibits spatial-temporal ET in close agreement with this gridded ET product.

The results from Figs. 2 and 3 demonstrate that CLM4 simulates the monthly and seasonal first layer soil moisture and evapotranspiration reasonably. The accuracy of

HESSD
11, 10431–10463, 2014

the estimated land surface states and fluxes therefore enables the use of the simulated variables in the diagnoses of the land–atmosphere coupling strength.

4.2 Background SM state

The sharp contrast in background SM state can be illustrated by taking a spatial-temporal average of SM as a function of depth for CTRL and DRY for DJF (Fig. 4a) and SON (Fig. 4b). The soil moisture away from the surface is markedly different between CTRL and DRY. During DJF, CTRL shows a slight increase in soil moisture with depth, reaching a peak of $\sim 0.35\,mm^3\,mm^{-3}$ at depths near 3 m. In contrast, DRY has a peak soil moisture of only $\sim 0.24\,mm^3\,mm^{-3}$ at the surface and decreases with depth to near zero at 3 m. Similar patterns of SM with depth are seen over SON, however SM_1 is considerably lower for both CTRL and DRY compared to DJF.

Despite the similar mean and temporal behavior of SM_1 shown in Fig. 2, SM away from the surface differs substantially between the two model configurations. The mean DJF ET is similar between CTRL and DRY, indicating that the surface evaporation is the dominant ET mechanism. The enhanced mean SM in CTRL causes the CTRL ET to be greater than the DRY ET during DJF, however both compare reasonable well to the observations (Fig. 3). However the lack of SM at depths below several centimeters for DRY during SON causes the reduced ET as compared to CTRL during this period. The mean ET during SON is sensitive to the mean SM away from the surface, indicating that transpiration significantly contributes to the total ET during this period. The reduced root zone SM in DRY leads to an increase in water stress and reduced transpiration. This reduction during SON is large relative to the mean ET during the period (Fig. 3).

4.3 Coupling strength: EF–LCL and SM_1–LCL

The statistical association between the evaporative fraction and the LCL is shown in Fig. 5. During DJF, CTRL (Fig. 5a) and DRY (Fig. 5c) exhibit strong surface flux-atmosphere coupling, with the strongest coupling over the Cape York Peninsula (East

HESSD
11, 10431–10463, 2014

of 140° E and North of 17° S) and the Southeastern part of the domain. Similarly, the EF–LCL coupling is significant during SON (Fig. 5b and d) over much of the domain, although the magnitude is reduced relative to DJF. Both ensembles show strong coupling independent of the season, however the differences between CTRL and DRY vary with season. DRY is generally more strongly coupled than CTRL during DJF (Fig. 5a and c), contrasting the similar coupling strength exhibited by both DRY and CTRL in SON (Fig. 5b and d). The reduced deep layer soil moisture resulting from the removal of the groundwater module enhances the DJF coupling while suppressing the SON coupling.

Figure 6 shows the median Kendall tau ($K\tau$) between SM_1 and the LCL (see Sect. 3.3) for CTRL and DRY separately during DJF (Fig. 6a and c) and SON (Fig. 6b and d). Several important features are present in Fig. 6. The SM_1–LCL coupling during DJF and SON is largely similar between the two model configurations. CTRL (Fig. 6a) and DRY (Fig. 6c) exhibit similar spatial patterns and magnitudes of $K\tau$. Small regions exhibit increases in the magnitude of $K\tau$ in CTRL relative to DRY in DJF (Fig. 6a and c) although the differences are statistically insignificant over most of the domain. Regardless of these slight variations in $K\tau$, CTRL and DRY exhibit a strongly coupled relationship between SM_1 and the boundary layer during the peak of the wet season over coincident parts of the domain. Both model configurations also show areas with insignificant coupling adjacent to the strongly coupled regions. In contrast, CTRL and DRY both contain regions of significant positive $K\tau$ demonstrating a negative coupling during SON. The similarity in SM_1–LCL coupling between CTRL and DRY during both DJF and SON implies that the temporal variability of SM_1 is physically independent of the season mean ET fluxes (Fig. 3).

Contrasting Figs. 5 and 6 reveals that the surface fluxes (Fig. 5b and d) are coupled despite the surface layer soil moisture (Fig. 6b and d) lacking similar coupling. The regions of positive $K\tau$ in Fig. 6 contradict the strongly negative $K\tau$ in Fig. 5 during SON. Similarly, the EF–LCL coupling during DJF is much stronger that the SM_1 coupling, and DRY generally exhibits stronger coupling than CTRL. In contrast, during SON, CTRL

HESSD
11, 10431–10463, 2014

generally shows slightly higher coupling strength than DRY (Fig. 6b and d), however the difference is not statistically significant over much of the domain. The change in sign of $K\tau$ from SON to DJF (Fig. 6b and d) demonstrates that applying Eq. (4) to SM_1 and the LCL does not always capture the coupling between the land and the atmosphere during periods where deep SM and transpiration dominate the ET flux.

In short, our results demonstrate that the surface layer soil moisture cannot adequately capture the SM-LCL coupling during both DJF and SON. The significant contributions of transpiration to the total ET fluxes (especially during SON) are responsive to perturbations in SM_{rz} and not SM_1.

4.4 Proposed coupling strength definition: SM_{rz}–LCL

The definition of land–atmosphere coupling using land surface moisture states and fluxes must encompass the relevant physical mechanisms. Previously, Ferguson et al. (2012) was limited to using SM_1 in deriving $K\tau$ because the AMSR-E (or other microwave) SM measurements only typically measure to depths less than a few centimeters beneath the soil surface. Computing $K\tau$ between SM_1 and the LCL incorporates the surface layer soil moisture that is important for surface evaporation from the soil. Therefore the DJF coupling (or other periods where the ET is mostly comprised of soil evaporation) should be adequately defined using SM_1. $K\tau$ computed from SM_1 neglects SM_{rz} variations that drive transpiration during the initial increase in precipitation following the dry season and therefore may not fully encompass the extent of land–atmosphere coupling. Acknowledging the importance of transpiration during the Northern Australian wet season, we further evaluate the land–atmosphere coupling by computing $K\tau$ between the vertically averaged SM_{rz} and the LCL. As opposed to remotely sensed SM from AMSR-E (or other satellite products), the use of simulated SM facilitates the estimation of SM_{rz}. Applying Eq. (4) using SM_{rz} imposes a different set of problems, as the rooting depth is model dependent and generally only approximately known. We assume that the SM_{rz} consists of the soil layers between the surface and

HESSD
11, 10431–10463, 2014

a depth of 1 m, as greater than 90 % of the prescribed roots in CLM4 are within 1 m of the surface (Oleson et al., 2010).

Figure 7 shows the ensemble median coupling strength diagnosed between SM_{rz} and the LCL. Comparing Figs. 5 and 7 it is clear that including the portion of SM that partially controls transpiration increases the magnitude of the DJF coupling strength and eliminates the regions with statistically insignificant coupling (Fig. 6) despite soil evaporation dominating the simulated ET. Large differences between SM_{rz}–LCL and SM_1–LCL coupling also occurs during SON. Both CTRL and DRY show statistically significant SON coupling, with groundwater exerting no significant impact (Fig. 7b and d). Comparing Fig. 7b and d with Fig. 3b and d reveals that despite the impact of groundwater on the mean ET flux over SON, the mean state of the deep SM imparts little influence on the temporal dynamics of SM_{rz} in relation to the LCL. Neglecting the SM beneath the surface layer in the calculation of $K\tau$ results in a weak diagnosed coupling strength during DJF and SON because transpiration is partly governed by the water availability within the root zone. By defining coupling strength using SM_{rz} it is clear that the land is strongly coupled to the LCL during both DJF and SON. The coupling strength for the CTRL simulations is stronger when defined in this manner, although both sets of simulations still show SM_{rz} to be statistically associated to the LCL.

The standard deviation of the coupling strength between SM_{rz} and the LCL and between SM_1 and the LCL among the ensemble members is generally less than 0.15 (Fig. 8a–d). The variation among the ensemble members is smaller than the median coupling strength shown in Figs. 6 and 7. The coupling using SM_1 (Fig. 8c) show larger ensemble uncertainty near the coast centered around 135° E compared to the SM_{rz} coupling in DJF (Fig. 8a) and over the Cape York Peninsula in SON (Fig. 8a and b). Aside from the region near 15° S and 130° E during SON, the larger ensemble uncertainty is found when using SM_1 to define the coupling strength.

HESSD
11, 10431–10463, 2014

5 Discussion

The seasonal ET from CTRL, DRY, and the observations from DJF through SON provide insight into the mechanisms that limit the SON DRY ET. The ET from CTRL and DRY are similar (within ±10 %) during the large DJF precipitation forcing. The dry season commences between MAM and JJA (Fig. 1) resulting in increased vapor pressure deficit (VPD) between the vegetation and the atmosphere and increased photosynthetically active radiation (PAR). The changes in VPD and PAR promote increased transpiration from DJF through MAM, although the actual transpiration is also governed by SM_{rz}. Comparing Figs. 3 and 4 indicates that the DRY ET is relatively SM limited and unable to maintain ET similar in magnitude to CTRL and the observations during SON. Physically, the soil column-groundwater interactions parameterized in CTRL inhibit the large, ET limiting SM_{rz} reduction present in DRY.

The coupling between EF–LCL (Fig. 5) is similar for both model configurations despite the mean ET (Fig. 3) and SM (Fig. 4) differing considerably between CTRL and DRY. The similarity holds for both DJF and SON despite the differing background soil moisture states between the two periods. The results indicate that while the mean ET is a strong function of mean soil moisture, the SM-LCL coupling as diagnosed here is insensitive to the background state. The coincidence of the temporal variations in SM, EF, and LCL are demonstrated by the large values of $K\tau$. These seemingly counterintuitive results may be an artifact of using a rank correlation coefficient to determine the coupling strength. $K\tau$ only measures the temporal coincidence of the two time-series while neglecting the magnitude of these variations. Although $K\tau$ is largely independent to the background soil moisture state, alternative definitions of coupling may not remain as invariant.

While coupling in Fig. 5 is largely unaffected by the mean SM state, the mean ET flux is largely derived from deeper SM through transpiration during the onset of the wet season prior to DJF. Coupling under these conditions is poorly defined using SM_1. The strong EF–LCL coupling during SON and DJF highlights the inadequacy of coupling

HESSD
11, 10431–10463, 2014

diagnosed with SM_1. The physically improbable SM_1–LCL coupling varies from positive (Fig. 5b) to negative (Fig. 5a) as the wet season is established (Fig. 1). Despite the domain mean precipitation increasing from roughly zero to several mm day^{-1} during SON, $K\tau$ from SM_1–LCL exhibits both positive and negative coupling over this period. The transition from negligible (or positive) to strong land–atmosphere coupling during the wet season is an artifact resulting from the use of SM_1. Consistent coupling in general agreement with the EF–LCL dynamics throughout the wet season exists between SM_{rz}–LCL because transpiration is incorporated into the coupling diagnostic. The necessity of using SM_{rz} agrees with Lee et al. (2012) where transpiration was found to limit precipitation variability over tropical regions. The dominance of transpiration among the various ET components is not limited to Northern Australia or monsoon regions (Jasechko et al., 2013) highlighting the need to characterize land–atmosphere dynamics using SM well beneath the surface.

Statistically determining the coupling strength using only near surface variables from land surface model simulations of SM observations (i.e. Ferguson et al., 2013; Betts, 2004) is limited due to only examining a part of the full land–atmosphere coupling processes. While the LCL is an important determinant in the formation of precipitation, moisture convergence, upper level inversions, convective available potential energy, wind shear, and many other factors play important roles in the formation of convection. The coupling diagnosed in this study with Eq. (4) is by definition limited in scope to only part of the coupling continuum described in Eq. (1). Therefore coupling defined using these methods provides a necessary but not sufficient condition for strong land–atmosphere interactions between soil moisture and precipitation.

Our results likely extend to monsoonal regions beyond Northern Australia. GLACE (Koster et al., 2006) revealed multiple areas of strong land–atmosphere coupling coincide with major monsoon systems. The strong coupling during the wet season (September–February) diagnosed using SM_{rz} and $K\tau$ in our results qualitatively agrees with the strong coupling in monsoon regions from GLACE. The dry season antecedent to the large precipitation fluxes induces low evaporation while allowing deeply rooted

HESSD
11, 10431–10463, 2014

plants to transpire despite the prolonged dry period. These conditions over Northern Australia (Figs. 3 and 4) lead to transpiration dominating the ET flux during the onset of the wet season. Coupling diagnosed using $K\tau$ under these conditions must be defined using SM_{rz} rather than SM_1 to ensure the relevant pathways of the moisture fluxes are not neglected.

6 Conclusions

The land–atmosphere coupling strength is analyzed utilizing ensembles of land surface simulations and near surface atmospheric data. Using four forcing datasets, ensembles of CLM simulations over Northern Australia are performed, using configurations that either include or neglect soil column-groundwater interactions. The seasonal dynamics of the simulated SM_1 is insensitive to the mean soil moisture state and all simulations compare favorably with the AMSR-E soil moisture product. Further, the simulated ET from December to February is similar between the CTRL and DRY runs, with both configurations largely consistent with the DJF ET estimated from three gridded ET products.

The strength of the land–atmosphere coupling is diagnosed between both SM_1 and EF from the simulations and the LCL as calculated from the near surface atmospheric state. During the peak wet season strong SM_1-LCL and EF–LCL coupling are shown. The wet season onset (SON) shows strong EF–LCL coupling that contrasts the weak SM_1-LCL coupling demonstrating the SON coupling is not properly characterized with SM_1. The land–atmosphere interactions during periods with non-negligible transpiration necessitates the use of root zone soil moisture instead of the surface soil moisture to properly capture the physical processes. Properly defining the coupling with SM_{rz} differs considerably from the SM_1 diagnosed coupling and shows strong coupling throughout the wet season. The SM_{rz}–LCL coupling is consistent with that from EF–LCL.

HESSD
11, 10431–10463, 2014

Our results also show that the diagnosed land–atmosphere coupling is insensitive to the mean vertical profile of soil moisture. It is however, sensitive to the depth of the soil column considered. The implication of our findings therefore indicates a need to include the root zone in order capture periods when the ET is dominated by transpiration. We recommend that future studies of land–atmosphere coupling should include groundwater and focus on root zone soil moisture rather than surface layer soil moisture.

Acknowledgements. We acknowledge support from the Australian Research Council Super Science scheme (FS100100054). A. Pitman was also supported by the Australian Research Council Centre of Excellence for Climate System Science (CE110001028). J. Evans was supported by an Australian Research Council Future Fellowship (FT110100576). The GLDAS data used in this study were acquired as part of the NASA's Earth–Sun System Division and archived and distributed by the Goddard Earth Sciences (GES) Data and Information Services Center (DISC) Distributed Active Archive Center (DAAC). We also thank Diego Miralles for providing the GLEAM ET product.

References

Betts, A. K.: Land-surface-atmosphere coupling in observations and models, J. Adv. Model. Earth Syst., 1, 3, doi:10.3894/JAMES.2009.1.4, 2009.

Betts, A. K., Ball, J. H., Beljaars, A. C. M., Miller, M. J., and Viterbo, P. A.: The land surface-atmosphere interaction: a review based on observational and global modeling perspectives, J. Geophys. Res.-Atmos., 101, 7209–7225, doi:10.1029/95JD02135, 1996.

Betts, A. K., Helliker, B., and Berry, J.: Coupling between CO_2, water vapor, temperature, and radon and their fluxes in an idealized equilibrium boundary layer over land, J. Geophys. Res.-Atmos., 109, 7209–7225, doi:10.1029/2003JD004420, 2004.

Bosilovich, M. G., Chen, J., Robertson, F. R., and Adler, R. F.: Evaluation of global precipitation in reanalyses, J. Appl. Meteorol. Clim., 47, 2279–2299, 2008.

Decker, M. and Zeng, X.: Impact of modified Richards equation on global soil moisture simulation in the Community Land Model (CLM3.5), J. Adv. Model. Earth Syst., 1, 3, doi:10.3894/JAMES.2009.1.5, 2009.

HESSD
11, 10431–10463, 2014

Decker, M., Pitman, A., and Evans, J. P.: Groundwater constraints on simulated transpiration variability over Southeastern Australian forests, J. Hydrometeorol., 14, 543–559, 2013.
Decker, M., Pitman, A., and Evans, J. P.: Applying scaled vegetation greenness metrics to constrain simulated transpiration anomalies: a study over Australia, J. Hydrometeorol., 15, 1607–1623, 2014.
Dirmeyer, P. A., Gao, X., Zhao, M., Guo, Z., Oki, T., and Hanasaki, N.: GSWP-2: multimodel analysis and implications for our perception of the land surface, B. Am. Meteorol. Soc., 87, 1381–1397, doi:10.1175/BAMS-87-10-1381, 2006.
Draper, C. S., Walker, J. P., Steinle, P. J., de Jeu, R. A. M., and Holmes, T. R. H.: An evaluation of AMSR-E derived soil moisture over Australia, Remote Sens. Environ., 113, 703–710, 2009.
Eamus, D. and Froend, R.: Groundwater-dependent ecosystems: the where, what and why of GDEs, Aust. J. Bot., 54, 91–96, 2006.
Evans, J. P., Pitman, A. J., and Cruz, F. T.: Coupled atmospheric and land surface dynamics over southeast Australia: a review, analysis and identification of future research priorities, Int. J. Climatol., 31, 1758–1772, doi:10.1002/joc.2206, 2011.
Fan, Y., Miguez-Macho, G., Weaver, C. P., Walko, R., and Robock, A.: Incorporating water table dynamics in climate modeling: 1. Water table observations and equilibrium water table simulations, J. Geophys. Res.-Atmos., 112, D10125, doi:10.1029/2006JD008111, 2007.
Ferguson, C. R. and Wood, E. F.: Observing land–atmosphere interaction globally with satellite remote sensing, in: Proc. Earth Observation and Water Cycle Science Symp., Frascati, Italy, p. 8, 2009.
Ferguson, C. R., Wood, E. F., and Vinukollu, R. K.: A global intercomparison of modeled and observed land–atmosphere coupling, J. Hydrometeorol., 13, 749–784, doi:10.1175/JHM-D-11-0119.1, 2012.
Gedney, N. and Cox, P. M.: The sensitivity of global climate model simulations to the representation of soil moisture heterogeneity, J. Hydrometeorol., 4, 1265–1275, 2003.
Gentine, P., Entekhabi, D., and Polcher, J.: The diurnal behavior of evaporative fraction in the soil–vegetation–atmospheric boundary layer continuum, J. Hydrometeorol., 12, 1530–1546, 2011.
Gentine, P., Holtslag, A. A. M., D'Andrea, F., and Ek, M.: Surface and atmospheric controls on the onset of moist convection over land, J. Hydrometeorol., 14, 1443–1462, 2013.
Guo, Z., Dirmeyer, P. A., Koster, R. D., Bonan, G., Chan, E., Cox, P., Gordon, C. T., Kanae, S., Kowalczyk, E., Lawrence, D., Liu, P., Lu, C.-H., Malyshev, S., Mcavaney, B., Mcgregor,

HESSD
11, 10431–10463, 2014

J. L., Mitchell, K., Mocko, D., Oki, T., Oleson, K. W., Pitman, A., Sud, Y. C., Taylor, C. M., Verseghy, D., Vasic, R., Xue, Y., and Yamada, T.: GLACE: the global land–atmosphere coupling experiment. Part II: Analysis, J. Hydrometeorol., 7, 611–625, doi:10.1175/JHM511.1, 2006.

Hirsch, A., Kala, J., Pitman, A. J., Carouge, C., Evans, J. P., Haverd, V., and Mocko, D.: Impact of land surface initialisation approach on sub-seasonal forecast skill: a regional analysis in the Southern Hemisphere, J. Hydrometeorol., 15, 300–319, 2014.

Huffman, G. J., Bolvin, D. T., Nelkin, E. J., Wolff, D. B., Adler, R. F., Gu, G., Hong, Y., Bowman, K. P., and Stocker, E. F.: The TRMM Multisatellite Precipitation Analysis (TMPA): quasi-global, multiyear, combined-sensor precipitation estimates at fine scales, J. Hydrometeorol., 8, 38–55, doi:10.1175/JHM560.1, 2007.

Jasechko, S., Sharp, Z. D., Gibson, J. J., Birks, S. J., Yi, Y., and Fawcett, P. J.: Terrestrial water fluxes dominated by transpiration, Nature, 496, 347–350, doi:10.1038/nature11983, 2013.

Jiménez, C., Prigent, C., Mueller, B., Seneviratne, S. I., McCabe, M. F., Wood, E. F., Rossow, W. B., Balsamo, G., Betts, A. K., Dirmeyer, P. A., Fisher, J. B., Jung, M., Kanamitsu, M., Reichle, R. H., Reichstein, M., Rodell, M., Sheffield, J., Tu, K., and Wang, K.: Global intercomparison of 12 land surface heat flux estimates, J. Geophys. Res., 116, D02102, doi:10.1029/2010JD014545, 2011.

Jones, D. A., Wang, W., and Fawcett, R.: High-quality spatial climate data-sets for Australia, J. Aust. Meteor. Oceanogr., 58, 233–248, 2009.

Jung, M., Reichstein, M., Ciais, P., Seneviratne, S. I., Sheffield, J., Goulden, M. L., Bonan, G., Cescatti, A., Chen, J., de Jeu, R., Dolman, A. J., Eugster, W., Gerten, D., Gianelle, D., Gobron, N., Heinke, J., Kimball, J., Law, B. E., Montagnani, L., Mu, Q., Mueller, B., Oleson, K., Papale, D., Richardson, A. D., Roupsard, O., Running, S., Tomelleri, E., Viovy, N., Weber, U., Williams, C., Wood, E., Zaehle, S., and Zhang, K.: Recent decline in the global land evapotranspiration trend due to limited moisture supply, Nature, 467, 951–954, doi:10.1038/nature09396, 2010.

Koster, R. D. and Suarez, M. J.: Impact of land surface initialization on seasonal precipitation and temperature prediction, J. Hydrometeorol., 4, 408–423, 2003.

Koster, R. D., Suarez, M. J., and Heiser, M.: Variance and predictability of precipitation at seasonal-to-interannual timescales, J. Hydrometeorol., 1, 26–46, 2000.

Koster, R. D., Guo, Z., Dirmeyer, P. A., Bonan, G., Chan, E., Cox, P., Davies, H., Gordon, C. T., Kanae, S., Kowalczyk, E., Lawrence, D., Liu, P., Lu, C.-H., Malyshev, S., Mcavaney, B.,

HESSD
11, 10431–10463, 2014

Mitchell, K., Mocko, D., Oki, T., Oleson, K. W., Pitman, A., Sud, Y. C., Taylor, C. M., Verseghy, D., Vasic, R., Xue, Y., and Yamada, T.: GLACE: the global land–atmosphere coupling experiment, Part I: Overview, J. Hydrometeorol., 7, 590–610, 2006.

Koster, R. D., Mahanama, S. P. P., Yamada, T. J., Balsamo, Gianpaolo, Berg, A. A., Boisserie, M., Dirmeyer, P. A., Doblas-Reyes, F. J., Drewitt, G., Gordon, C. T., Guo, Z., Jeong, J.-H., Lee, W.-S., Li, Z., Luo, L., Malyshev, S., Merryfield, W. J., Seneviratne, S. I., Stanelle, T., van den Hurk, B. J. J. M., Vitart, F., and Wood, E. F.: The second phase of the global land–atmosphere coupling experiment: soil moisture contributions to subseasonal forecast skill, J. Hydrometeorol., 12, 805–822, doi:10.1175/2011JHM1365.1, 2011.

Lee, J.-E., Lintner, B., Neelin, J. D., Jiang, X., Gentine, P., Boyce, C. K., Fisher, J. B., Perron, J. T., Kubar, T. L., Lee, J., and Worden, J. R.: Reduction of tropical land region precipitation variability via transpiration, Geophys. Res. Lett., 39, L19704, doi:10.1029/2012GL053417, 2012.

Lintner, B. R. and Neelin, J. D.: Soil moisture impacts on convective margins, J. Hydrometeorol., 10, 1026–1039, 2009.

Lintner, B. R., Gentine, P., Findell, K. L., D'Andrea, F., Sobel, A. H., and Salvucci, G. D.: An idealized prototype for large-scale land–atmosphere coupling, J. Climate, 26, 2379–2389, 2013.

Liu, Y. Y., van Dijk, A. I. J. M., De Jeu, R. A. M., and Holmes, T. R. H.: An analysis of spatiotemporal variations of soil and vegetation moisture from a 29-year satellite-derived data set over mainland Australia, Water Resour. Res., 45, W07405, doi:10.1029/2008WR007187, 2009.

Lo, M.-H. and Famiglietti, J. S.: Effect of water table dynamics on land surface hydrologic memory, J. Geophys. Res., 115, D22118, doi:10.1029/2010JD014191, 2010.

Meng, X. H., Evans, J. P., and McCabe, M. F.: The impact of observed vegetation changes on land–atmosphere feedbacks during drought, J. Hydrometeorol., 15, 759–776, doi:10.1175/JHM-D-13-0130.1, 2014.

Miralles, D. G., De Jeu, R. A. M., Gash, J. H., Holmes, T. R. H., and Dolman, A. J.: Magnitude and variability of land evaporation and its components at the global scale, Hydrol. Earth Syst. Sci., 15, 967–981, doi:10.5194/hess-15-967-2011, 2011a.

Miralles, D. G., Holmes, T. R. H., De Jeu, R. A. M., Gash, J. H., Meesters, A. G. C. A., and Dolman, A. J.: Global land-surface evaporation estimated from satellite-based observations, Hydrol. Earth Syst. Sci., 15, 453–469, doi:10.5194/hess-15-453-2011, 2011b.

HESSD
11, 10431–10463, 2014

Mu, Q., Heinsch, F. A., Zhao, M., and Running, S. W.: Development of a global evapotranspiration algorithm based on MODIS and global meteorology data, Remote Sens. Environ., 111, 519–536, doi:10.1016/j.rse.2007.04.015, 2007.

Mu, Q., Zhao, M., and Running, S. W.: Improvements to a MODIS global terrestrial evapotranspiration algorithm, Remote Sens. Environ., 115, 1781–1800, 2011.

Niu, G.-Y., Yang, Z.-L., Dickinson, R. E., Gulden, L. E., and Su, H.: Development of a simple groundwater model for use in climate models and evaluation with gravity recovery and climate experiment data, J. Geophys. Res.-Atmos., 112, D07103, doi:10.1029/2006JD007522, 2007.

Njoku, E. G., Jackson, T. J., Lakshmi, V., Chan, T. K., and Nghiem, S. V.: Soil moisture retrieval from AMSR-E, IEEE T. Geosci. Remote, 41, 215–229, doi:10.1109/TGRS.2002.808243, 2003.

Oleson, K. W., Lawrence, D. M., Bonan, G. B., Flanner, M. G., Kluzek, E., Lawrence, P. J., Levis, S., Swenson, S. C., Thornton, P. E., Dai, A., Decker, M., Dickinson, R., Feddema, J., Heald, C. L., Hoffman, F., Lamarque, J.-F., Mahowald, N., Niu, G.-Y., Qian, T., Randerson, J., Running, S., Sakaguchi, K., Slater, A., Stöckli, R., Wang, A., Yang, Z.-L., Zeng, X., and Zeng, X.: Technical Description of Version 4.0 of the Community Land Model (CLM), National Center for Atmospheric Research (NCAR), Boulder, Colorado, doi:10.5065/D6FB50WZ, 2010.

Pielke, R. A., Pitman, A., Niyogi, D., Mahmood, R., McAlpine, C., Hossain, F., Goldewijk, K. K., Nair, U., Betts, R., Fall, S., Reichstein, M., Kabat, P., and de Noblet, N.: Land use/land cover changes and climate: modeling analysis and observational evidence, WIREs Clim. Change, 2, 828–850, doi:10.1002/wcc.144, 2011.

Pitman, A. J.: The evolution of, and revolution in, land surface schemes designed for climate models, Int. J. Climatol., 23, 479–510, doi:10.1002/joc.893, 2003.

Press, W. H., Flannery, B. P., Teukolsky, S. A., and Vetterling, W. T.: Nonparametric or rank correlation, numerical recipes, in: C: the Art of Scientific Computing, 2nd Edn., edited by: Cowles, L. and Harvey, A., Cambridge University Press, 639–644, 1992.

Qian, T., Dai, A., Trenberth, K. E., and Oleson, K. W.: Simulation of global land surface conditions from 1948 to 2004, Part I: Forcing data and evaluations, J. Hydrometeorol., 7, 953–975, doi:10.1175/JHM540.1, 2006.

Reichle, R. H. and Koster, R. D.: Bias reduction in short records of satellite soil moisture, Geophys. Res. Lett., 31, L19501, doi:10.1029/2004GL020938, 2004.

HESSD
11, 10431–10463, 2014

Rodell, M., Houser, P. R., Jambor, U., Gottschalck, J., Mitchell, K., Meng, C.-J., Arsenault, K., Cosgrove, B., Radakovich, J., Bosilovich, M., Entin, J. K., Walker, J. P., Lohmann, D., and Toll, D.: The global land data assimilation system, B. Am. Meteorol. Soc., 85, 381–394, doi:10.1175/BAMS-85-3-381, 2004.

Santanello, J. A., Peters-Lidard, C. D., and Kumar, S. V.: Diagnosing the sensitivity of local land–atmosphere coupling via the soil moisture-boundary layer interaction, J. Hydrometeorol., 12, 766–786, doi:10.1175/JHM-D-10-05014.1, 2011.

Seneviratne, S. I., Corti, T., Davin, E. L., Hirschi, M., Jaeger, E. B., Lehner, I., Orlowsky, B., and Teuling, A. J.: Investigating soil moisture-climate interactions in a changing climate: a review, Earth-Sci. Rev., 99, 125–161, doi:10.1016/j.earscirev.2010.02.004, 2010.

Small, E. E. and Kurc, S. A.: Tight coupling between soil moisture and the surface radiation budget in semiarid environments: implications for land–atmosphere interactions, Water Resour. Res., 39, 1278, doi:10.1029/2002WR001297, 2003,

Taylor, C. M. and Ellis, R. J.: Satellite detection of soil moisture impacts on convection at the mesoscale, Geophys. Res. Lett., 33, L03404, doi:10.1029/2005GL025252, 2006.

Vergnes, J.-P., Decharme, B., Alkama, R., Martin, E., Habets, F., and Douville, H.: A simple groundwater scheme for hydrological and climate applications: description and offline evaluation over France, J. Hydrometeorol., 13, 1149–1171, doi:10.1175/JHM-D-11-0149.1, 2012.

Westra, D., Steeneveld, G. J., and Holstag, A. A. M.: Some observational evidence for dry soils supporting enhanced relative humidity at the convective boundary layer top, J. Hydrometeorol., 13, 1347–1358, 2012.

Williams, J. L. and Maxwell, R. M.: Propagating subsurface uncertainty to the atmosphere using fully coupled stochastic simulations, J. Hydrometeorol., 12, 690–701, doi:10.1175/2011JHM1363.1, 2011.

Yu, Z., Pollard, D., and Cheng, L.: On continental-scale hydrologic simulations with a coupled hydrologic model, J. Hydrol., 331, 110–124, doi:10.1016/j.jhydrol.2006.05.021, 2006.

Zeng, X. and Decker, M.: Improving the numerical solution of soil moisture-based Richards equation for land models with a deep or shallow water table, J. Hydrometeorol., 10, 308–319, 2009.

Zhang, J., Wang, W.-C., and Wei, J.: Assessing land–atmosphere coupling using soil moisture from the global land data assimilation system and observational precipitation, J. Geophys. Res.-Atmos., 113, D17119, doi:10.1029/2008JD009807, 2008.

HESSD
11, 10431–10463, 2014

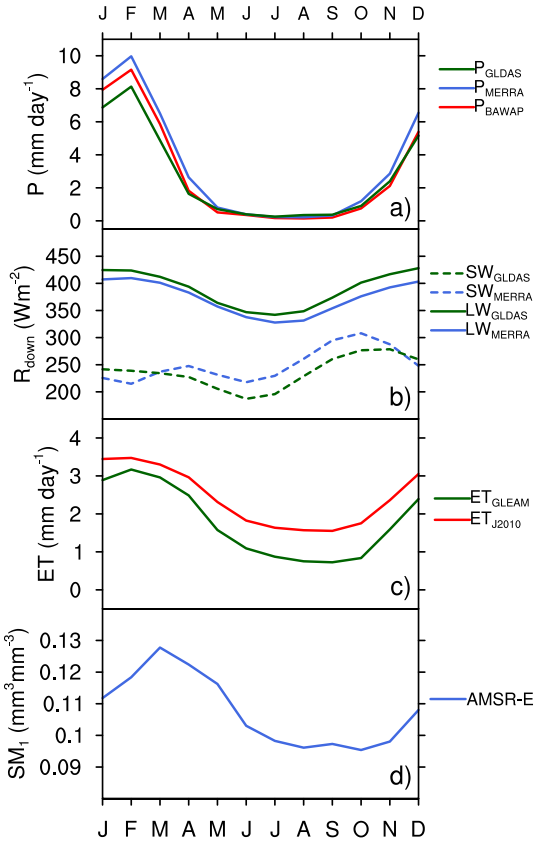

Figure 1. Observations of the domain (18° S–11° S and 120° E–150° E) averaged mean annual cycle of **(a)** precipitation (P in mm day^{-1}), **(b)** longwave (LW) and shortwave (SW) downward radiative (R_{down}) forcing (W m^{-2}), **(c)** evapotranspiration (ET in mm day^{-1}), and surface layer soil moisture (SM_1 in mm^3 mm^{-3}).

HESSD
11, 10431–10463, 2014

Diagnosing the seasonal land–atmosphere coupling strength over Australia

M. Decker et al.

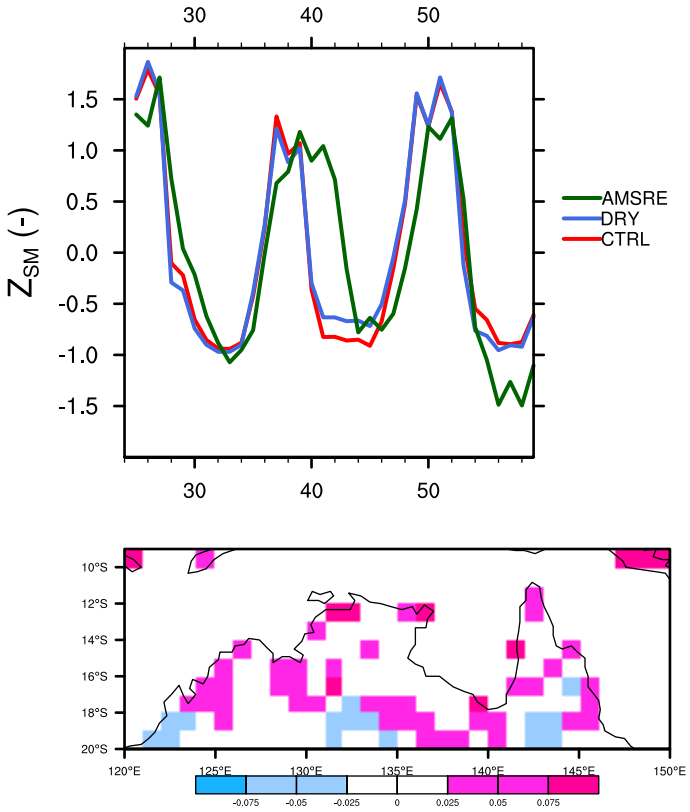

Figure 2. (a) The mean normalized first layer soil moisture (SM1) from the CTRL and DRY simulations and the AMSR-E observations. **(b)** The difference between the mean SM_1 (from all simulations) and the AMSR-E observations.

HESSD
11, 10431–10463, 2014

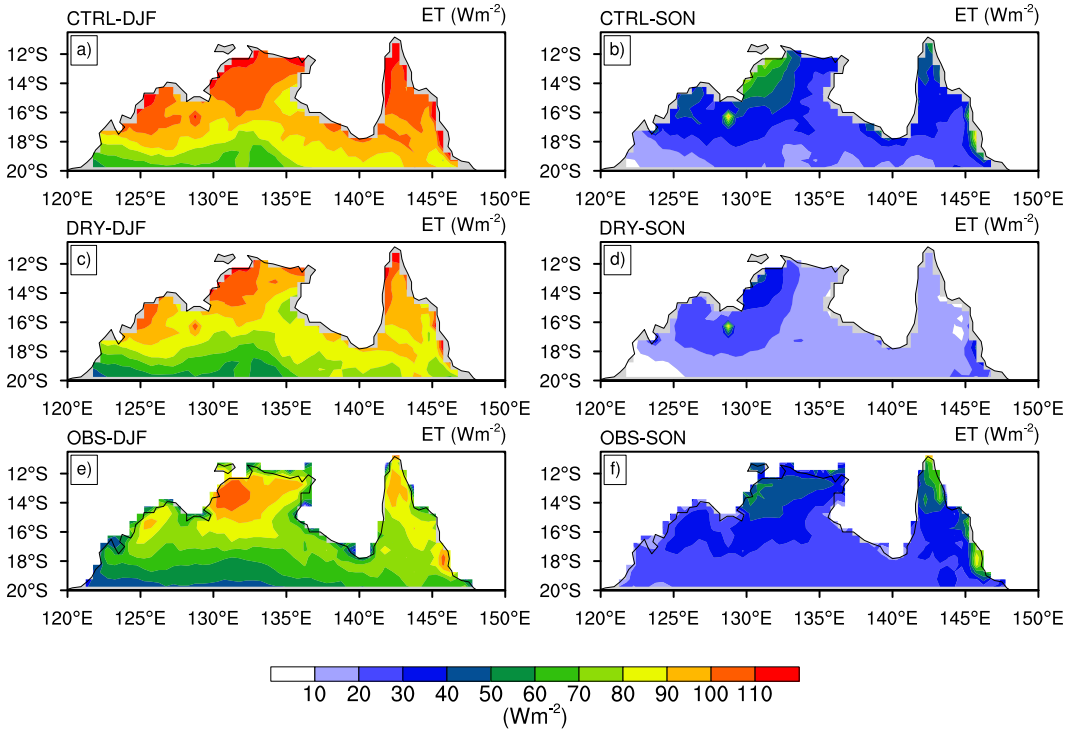

Figure 3. The mean ET ($W\,m^{-2}$) from the wet season (DJF shown in the left hand column) and the transition between the dry and wet seasons (SON shown in the right hand column). The ensemble mean ET from **(a)** CTRL over DJF, **(b)** CTRL over SON, **(c)** DRY for DJF, **(d)** DRY from SON, **(e)** OBS (the mean of three gridded ET products) over DJF, and **(f)** OBS for SON.

HESSD
11, 10431–10463, 2014

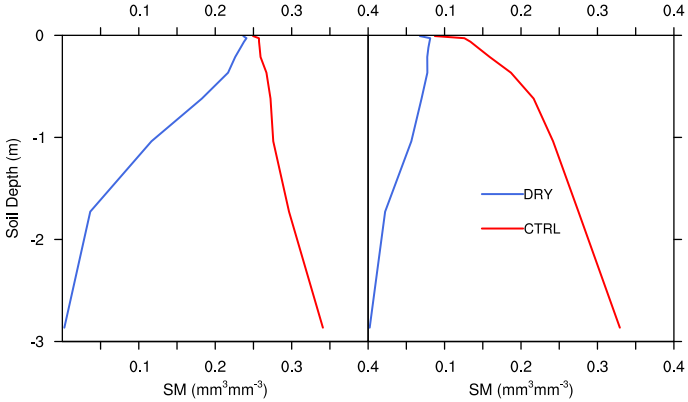

Figure 4. Spatiotemporal mean soil moisture ($mm^3\,mm^{-3}$) SM as a function of depth (m) for DJF (left panel) and SON (right panel).

HESSD
11, 10431–10463, 2014

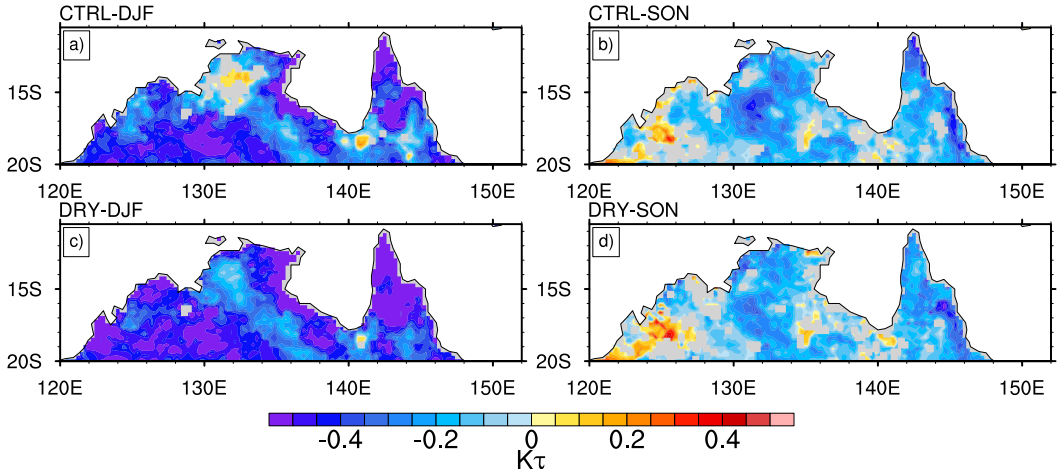

Figure 5. The ensemble median Kendall-tau correlation metric ($K\tau$) between the morning time (local) evaporative fraction (EF) and the afternoon computed lifting condensation level (LCL) at from **(a)** CTRL over DJF, **(b)** CTRL from SON, **(c)** DRY over DJF, and **(d)** DRY from SON. Only statistically significant (95 % confidence level) results are shown in **(a–d)**.

HESSD
11, 10431–10463, 2014

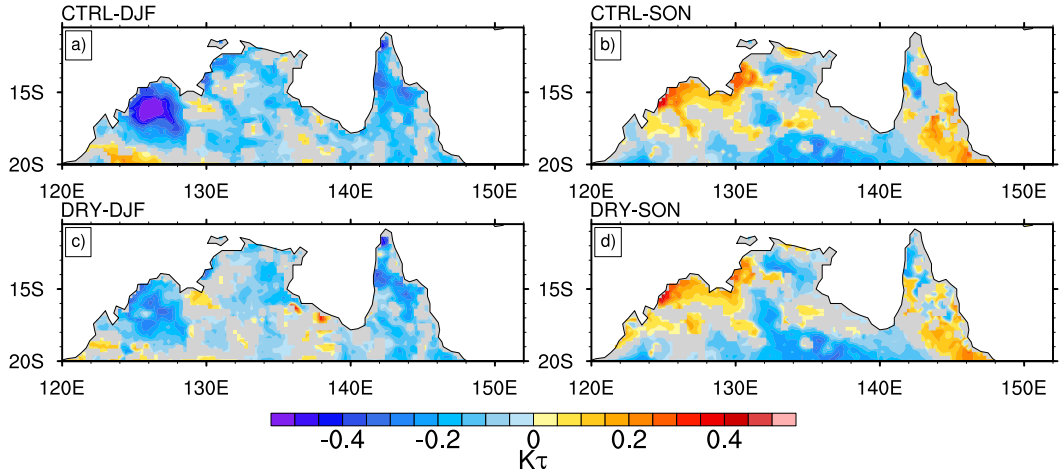

Figure 6. The ensemble median Kendall-tau correlation metric ($K\tau$) between the morning first layer soil moisture (SM_1) and the afternoon computed lifting condensation level (LCL) from **(a)** CTRL over DJF, **(b)** CTRL from SON, **(c)** DRY over DJF, and **(d)** DRY from SON. Only statistically significant (95 % confidence level) results are shown in **(a)**–**(d)**.

HESSD
11, 10431–10463, 2014

Diagnosing the seasonal land–atmosphere coupling strength over Australia

M. Decker et al.

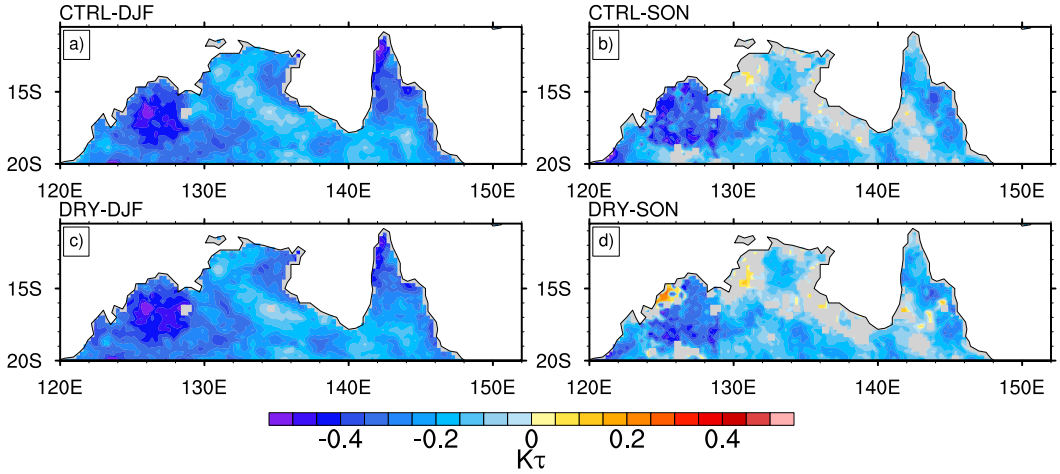

Figure 7. The ensemble median Kendall-tau correlation metric ($K\tau$) between the morning root zone soil moisture (SM_{rz}) and the afternoon computed lifting condensation level (LCL) from **(a)** CTRL over DJF, **(b)** CTRL from SON, **(c)** DRY over DJF, and **(d)** DRY from SON. Only statistically significant (95 % confidence level) results are shown in **(a)**–**(d)**.

HESSD
11, 10431–10463, 2014

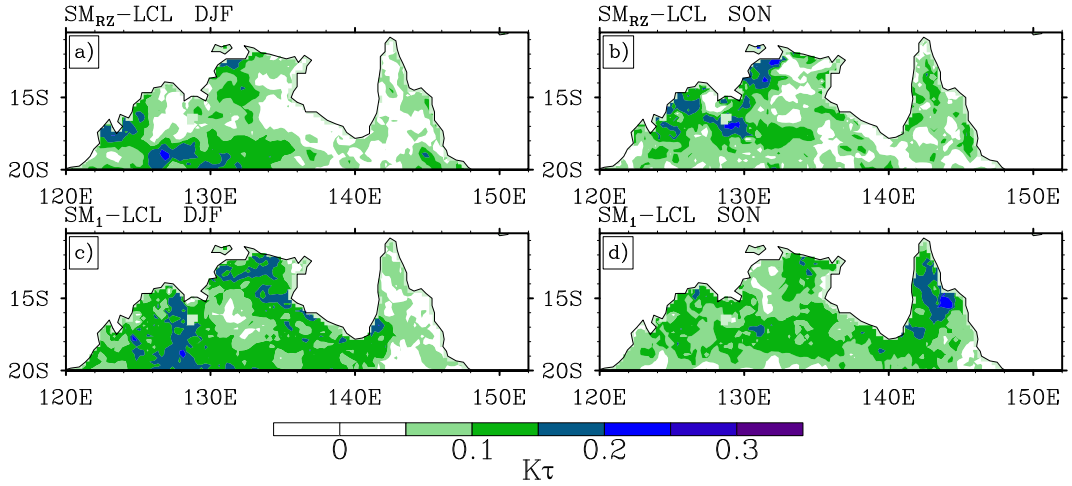

Figure 8. The standard deviation of the Kendall-tau correlation metric ($K\tau$) among the ensemble members between the afternoon computed lifting condensation level (LCL) and either the morning root zone soil moisture (SM_{rz}) over **(a)** DJF, **(b)** SON, or the morning first layer soil moisture (SM_1) over **(c)** DJF, and **(d)** SON.

HESSD
11, 10431–10463, 2014